Low-energy elastic electron scattering from furan

M. A. Khakoo,[1,*] J. Muse,[1] K. Ralphs,[1] R. F. da Costa,[2] M. H. F. Bettega,[3] and M. A. P. Lima[4,5]

[1]*Department of Physics, California State University, Fullerton, California 92834, USA.*

[2]*Centro de Ciências Naturais e Humanas, Universidade Federal do ABC, 09210-170 Santo André, São Paulo, Brazil*

[3]*Departamento de Física, Universidade Federal do Paraná, Caixa Postal 19044, 81531-990 Curitiba, Paraná, Brazil*

[4]*Instituto de Física "Gleb Wataghin," Universidade Estadual de Campinas, Caixa Postal 6165, 13083-970 Campinas, São Paulo, Brazil*

[5]*Laboratório Nacional de Ciência e Tecnologia do Bioetanol (CTBE), Centro Nacional de Pesquisa em Energia e Materiais (CNPEM), Caixa Postal 6170, 13083-970 Campinas, São Paulo, Brazil*

(Received 5 May 2010; published 30 June 2010)

We report normalized experimental and theoretical differential cross sections for elastic electron scattering by C_4H_4O (furan) molecules from a collaborative project between several Brazilian theoretical groups and an experimental group at California State Fullerton, USA. The measurements are obtained by using the relative flow method with helium as the standard gas and a thin aperture target gas collimating source. The relative flow method is applied without the restriction imposed by the relative flow pressure condition on helium and the unknown gas. The experimental data were taken at incident electron energies of 1, 1.5, 1.73, 2, 2.7, 3, 5, 7, 10, 20, 30, and 50 eV and covered the angular range between 10° and 130°. The measurements verify observed π^* shape resonances at 1.65 ± 0.05eV and 3.10 ± 0.05 eV scattering energies, in good agreement with the transmission electron data of Modelli and Burrow [J. Phys. Chem. A **108**, 5721 (2004)]. Furthermore, the present results also indicated both resonances dominantly in the *d*-wave channel. The differential cross sections are integrated in the standard way to obtain integral elastic cross sections and momentum transfer cross sections. The calculations employed the Schwinger multichannel method with pseudopotentials and were performed in the static-exchange and in the static-exchange plus polarization approximations. The calculated integral and momentum transfer cross sections clearly revealed the presence of two shape resonances located at 1.95 and 3.56 eV and ascribed to the B_1 and A_2 symmetries of the C_{2v} point group, respectively, in very good agreement with the experimental findings. Overall agreement between theory and experiment regarding the differential, momentum transfer, and integral cross sections is very good, especially for energies below 10 eV.

DOI: 10.1103/PhysRevA.81.062716 PACS number(s): 34.80.Gs, 34.80.Bm

I. INTRODUCTION

This study and many such investigations are motivated by the seminal work of Sanche and co-workers [1]. These authors experimentally demonstrated that single-strand and double-strand breaks in DNA, induced by secondary low-energy electrons (below 20 eV), play a dominant role for the understanding of the damage effects of ionizing radiation in living cells and tissues. This discovery has stimulated strong interest concerning the scattering of slow electrons by biologically relevant molecules. Much ongoing effort has been undertaken by theoretical and experimental groups to provide a deeper insight into the mechanisms related to the radiation damage of DNA, which includes both direct processes (ionization, electronic, rotational, and vibrational excitations) as well as compound processes such as resonances (dissociation and dissociative electron attachment). These studies can be generally grouped according to one of the following research fronts: (i) those involving structural units of the DNA, such as the phosphate group, the deoxyribose sugar, the nucleic acid bases, or some of its fragments [2–6]; (ii) those involving other molecules carrying structural or functional properties similar to those of small parts of the DNA [7–10], and (iii) the investigation of the effect of water in the location of a π^* shape resonance in small molecules, such as formaldehyde [11]. A particular feature that many among these molecules have in common is the presence of a first excited triplet state lying at around 3 to 4 eV [12] above the ground state. Relevant within this context and also well recognized is the fact that at this range of electron impact energies, the inclusion of polarization effects is very important for an accurate description of the scattering process, especially with regard to the determination of the resonances' positions. Taking the above considerations in mind, we chose this molecule (C_4H_4O) because it represents a simpler but similar system to the tetrahydrofuran molecule (C_4H_8O), a sugar-like component of the backbone of the DNA, and also because it presents two prominent shape resonances around the $^3B_2$ excitation threshold [10,13–15]. Theoretical calculations on electron collisions with furan were recently performed by Bettega and Lima [10] and by da Costa and co-workers [16] and revealed the importance of inclusion of polarization effects in the description of elastic as well as electronically inelastic processes, respectively. Whereas furan has not been experimentally investigated, a closely related molecule to it, tetrahydrofuran (THF), has been studied in the gas phase by several groups [14,17–19] most recent being that of Allan [19]. Different theoretical methods and approaches also addressed elastic and inelastic electron scattering by THF [3,6,7,20,21]. Although these molecules are quite similar from a structural standpoint, it should be noted that tetrahydrofuran has a much larger dipole moment (1.70 D) [22] than that of furan (0.67 D) [22,23]. Further, it does not have the π-double bond cyclic structure whereas furan does. Thus the expected

*mkhakoo@fullerton.edu

resonant structure based on dissociative electron attachment to π-double bonds, absent in tetyrahydrofuran, should be present in furan, which is a point of interest in this work.

The paper is organized as follows. In Secs. II and III we describe the apparatus and techniques used to obtain the experimental data and the most relevant aspects related to the scattering calculations, respectively. In Sec. IV, measured and calculated cross sections are presented and critically compared with each other. Conclusions are summarized in Sec. V.

II. EXPERIMENTAL

The experimental apparatus has been described in previous articles (e.g., Khakoo and co-workers [24]) so only a brief description will be given here. The electron gun and the detector employ double hemispherical energy selectors, and the apparatus is made of titanium. Cylindrical lenses are used, and the system was baked to about 130°C with magnetically free biaxial heaters (ARi Industries model BXX06B41–4 K). The analyzer detector was a discrete dynode electron multiplier (Equipe Thermodynamique et Plasmasmodel AF151) with the extremely low background rate of <0.01 Hz and the capability of linearly detecting up to 1 MHz of electrons without saturating. The remnant magnetic field in the collision region is reduced to less than 1 mG by using a double μ-metal shield as well as a coil that eliminates the vertical component of the Earth's magnetic field. Typical electron currents were around 15 to 30 nA, with an energy resolution of 50 to 80 meV, full width at half maximum. The larger current is more desirable at higher-incident electron energies (E_0). The electron beam could be easily focused at 1 eV and remained stable to within 20% over a period of several days, requiring minor tuning of the spectrometer to maintain the long-term stability of the current to within 5%. The energy of the beam was established by determining the dip in the He elastic-scattering cross section due to the $2\,^2S$ He^- resonance at 19.366 eV [25] to an uncertainty of ±20 meV during a run at a given impact energy E_0. Typically the contact potential so determined drifted at around 0.8 to 0.9 eV over the multiweek course of the experiments. Energy-loss spectra of the elastic peak were collected at fixed E_0 values and electron scattering angles θ by repetitive, multichannel-scaling techniques. The angular resolution was 2°, full width at half maximum. The effusive target gas beam was formed by flowing gas through a thin aperture source 0.3 mm in diameter described previously [26]. This source was sooted, using an acetylene flame, to reduce secondary electrons and placed 6 mm below the axis of the electron beam, incorporated into a movable source arrangement [27]. The movable gas source method has been well tested previously in our laboratory and determines background scattering rates expediently and accurately. The vapor pressure behind the source for furan or helium was about 0.14 or 1 Torr, respectively, and the pressure in the experimental chamber $\sim 1 \times 10^{-6}$ Torr. The gas beam temperature, determined by the apparatus temperature in the collision region, was about 130°C, however, in most of the gas handling copper tubing the temperature was 24°C. The higher temperature was in the last 4 cm of the gas handling system before the gas exited into the collision region. Based on the flow-rate versus drive pressure analysis [26], the gas kinetic molecular diameter of furan was determined to be 5.24×10^{-8} cm, which is a significantly larger molecular diameter than that quoted by [19,28] for tetrahydrofuran of 4.68×10^{-8} cm. Based on the fact that the dipole moment of tetrahydrofuran exceeds that of furan by a factor of 2.5, and is a larger more massive structure than furan, one could expect the molecular diameter of tetrahydrofuran to be greater than the quoted values in [19,28], roughly closer to, in our estimate, 6×10^{-8} cm.

Our elastic scattering measurements were taken at E_0 values of 1, 1.5, 1.73, 2, 2.7, 3, 5, 7, 10, 20, 30, and 50 eV for scattering angles ranging from 10° to 130° as described in [26]. To compute momentum-transfer and integral elastic cross sections, the measured differential cross sections (DCS's) were extrapolated to 0° and 180° using theory as an aid wherever possible. The extrapolation at forward angles at low E_0 used the Born-dipole form of the DCS with a dipole moment of 0.685 Debye (D) and a rotational energy loss of 5 meV [24], below $E_0 = 2.5$ eV and theory for energies above this.

III. THEORETICAL

To compute the scattering cross sections we employed the Schwinger multichannel (SMC) method [29] implemented with pseudopotentials (SMCPP) [30]. The theoretical approach and the computational details applied in this study are essentially the same as those used in our previous works and therefore, here we just outline the aspects that are relevant to the present calculations.

The target molecule is represented at the restricted Hartree-Fock (HF) level of approximation with the nuclei fixed at the ground-state equilibrium geometry. In both bound state and scattering calculations we used the local-density norm-conserving pseudopotentials of Bachelet and co-workers [31] to represent the nuclei and the core electrons of each atom, except for hydrogen. The basis set used in these calculations is $5s5p2d$ on each carbon and oxygen as listed in Table I, obtained according to a variational method [32], and the basis set for hydrogen is Dunning's $4s/3s$ set augmented with one p-type function with the exponent equal to 0.75. The HF equilibrium geometry shown in Fig. 1, on the other hand, was obtained

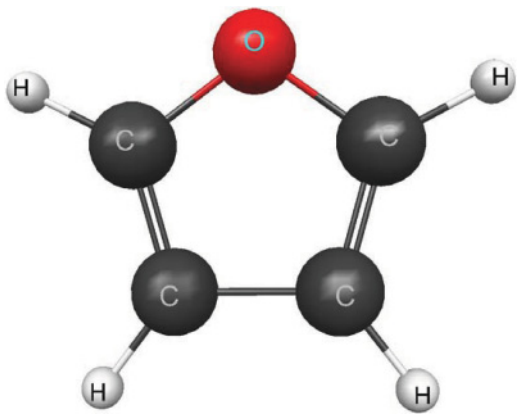

FIG. 1. (Color online) Geometrical structure of furan (generated with MacMolPlot [33]).

TABLE I. Uncontracted Cartesian Gaussian functions used for carbon and oxygen.

Type	Carbon Exponent	Oxygen Exponent
s	12.49628	16.05878
s	2.470286	5.920242
s	0.614028	1.034907
s	0.184028	0.316843
s	0.039982	0.065203
p	5.228869	10.14127
p	1.592058	2.783023
p	0.568612	0.84101
p	0.210326	0.23294
p	0.07225	0.052211
d	0.603592	0.756793
d	0.156753	0.180759

with the GAMESS package [34] employing the 6–31(d) basis set, with the target treated as a C_{2v} molecule.

Our calculations were performed in the static-exchange (SE) and in the static-exchange plus polarization (SEP) approximations. The scattering amplitudes are obtained within the minimal orbital basis for single configuration interactions (MOB-SCI) approach [35] for electron impact energies up to 50 eV. To represent polarization effects we considered single excitations from the occupied molecular orbitals to a set of modified virtual orbitals (MVO's) [36] obtained through the diagonalization of a Fock operator of a cation with charge +2. We retained only the MVO's with energies less than 10 Hartrees and used this same set of MVO's to represent the scattering orbitals. We considered singlet-coupled and triplet-coupled excitations and obtained 4878 $(N+1)$-electron doublet configuration state functions (CSF's) for the A_1 symmetry, 4391 CSF's for B_1, 4879 CSF's for B_2, and 4383 CSF's for A_2.

The computed value of the permanent dipole moment for furan was 0.85 D, being in relative good agreement with the published experimental values of 0.67 D [22,23]. The correction due to the long-range character of the dipole interaction were explicitly accounted for in our calculations through the Born closure procedure usually applied in the treatment of electron scattering by polar molecules [37]. In short, the procedure can be described as follows. Present elastic scattering amplitudes were calculated in the body reference frame (BF) of the molecular target. In that frame we also calculated the first-Born approximation (FBA) to the scattering amplitude for a point-dipole potential with the same orientation and magnitude as the molecular dipole used in the SMCPP calculation. These two amplitudes were then expanded into partial waves up to a maximum electronic orbital angular momentum $\ell_{\max}$, subtracted from each other ($F_{\rm diff}^{\rm body} = F_{\rm SMCPP} - F_{\rm dipole}$) and transformed into the laboratory frame, giving rise to $F_{\rm diff}^{\rm lab}$, where the z axis is along the incident wave direction. In the laboratory frame a closed form of the point-dipole amplitude can be obtained in the FBA and added to the resulting amplitude (i.e., $F_{\rm dipole}^{\rm lab} + F_{\rm diff}^{\rm lab}$). In summary, this procedure corresponds to simply replacing the low partial waves of the full point-dipole amplitude obtained in the FBA by the SMCPP partial waves. The highest angular momenta computed with the SMCPP method in the present SEP calculations were $\ell_{\max} = 3$ at 1, 1.5, and 1.7 eV, $\ell_{\max} = 4$ at 2.7, 3.0, 3.5, and 5.0 eV, $\ell_{\max} = 5$ at 10 eV, and finally, $\ell_{\max} = 10$ at 20 eV. These values were chosen to provide the best matching between the differential cross sections obtained with and without the Born closure for scattering angles above 40°.

The numerical stability of the calculations presented in this paper was checked with the procedure developed by Chaudhuri and co-workers, as adapted to electron-molecule scattering problem [35]. This procedure has been successfully applied to the analysis of spurious structures arising from numerical linear dependence among basis set functions in a series of recent applications of the SMC method.

IV. RESULTS AND DISCUSSION

Our experimental and theoretical DCS's are summarized in Fig. 2. Measured DCS's were thus integrated in the standard way [26] to obtain integral cross sections (ICS) and momentum-transfer cross sections (MTCS), which are plotted with the corresponding calculated cross sections in Fig. 3. We note here that the experimental results do exclude excitation of vibrational modes with energies below 30 meV, and such features did not contribute to more than 10% of the energy loss spectra. In Fig. 4, the results of scanning the energy of the electron beam, but fixing the scattering angle at 90° are plotted along with the experimental and theoretical DCS's in an effort to locate the positions of the negative ion resonances.

From the results shown in Fig. 2 the dominating role of the long-range dipole interaction between the target and incoming electron for small θ, especially at lower energies becomes clear. For example, at $E_0 = 1$ eV the SMCPP result without the Born-dipole correction agrees very well with the experimental DCS's at large and intermediate angles, but has to have the Born dipole included to improve the agreement at $\theta < 50°$. At higher energy values, more specifically from $E_0 = 1.73$ up to 10 eV, agreement between calculated and measured cross sections is very good both in terms of absolute values as in terms of shape. For example, at 5 and 10 eV the agreement is excellent, and reinforces the fact that the aperture source method is able to make accurate quantitative measurements of elastic scattering without requiring the knowledge of gas kinetic cross sections (see also Ref. [26]). At $E_0 = 20$ eV the SMCPP result overestimates the experimental DCS, but gives a good qualitative shape. However, not shown here, this agreement progressively gets worse at higher E_0 values since the reliability of the DCS's obtained at the SEP level of approximation is limited to lower E_0 values where excitation and ionization channels are not important. Indeed, as the incident electron energy increases the inclusion of these inelastic channels is essential since the competition among all energetically accessible states properly accounts for flux which, in turn, should lead to a reduction in the magnitude of calculated cross sections. This effect was, in fact, observed in recent investigations on elastic electron-molecule collisions where inclusion of a complex optical potential representing the inelastic channels improved the agreement between calculated

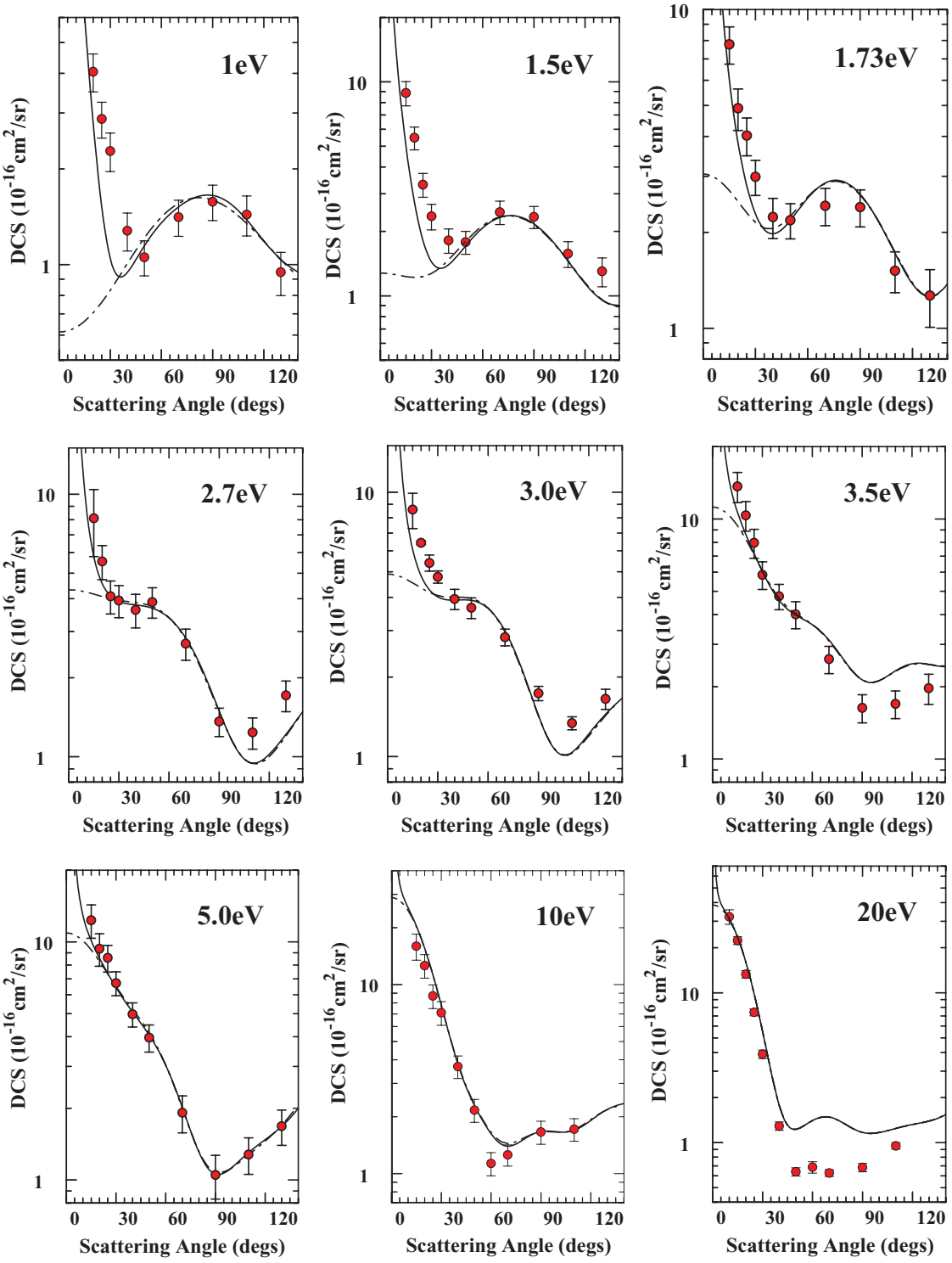

FIG. 2. (Color online) Elastic electron scattering DCS's for furan at various E_0 values. The circles are the present experiment with 1 standard deviation errors; solid black line is the theory, SMCPP with Born-closure (BC) procedure; and the dot dashed line is the SMCPP without BC procedure.

and measured DCS at intermediate angles (see, for instance, Refs. [38,39] and references therein).

We also observe the strong d-wave profile of the scattering at the resonant energy of 1.73 eV for the π^* (B_1) resonance, first experimentally detected by Modelli and Burrow [13]. However, fitting this profile with a theoretical angular distribution given by Read [40] is complicated by the strong forward dipole scattering. Nevertheless the peak at $\theta = 90^\circ$ is found to be fully developed at $E_0 = 1.73$ eV in a clearer way than for the π^* (A_2) resonance at 3.15 eV [13]. For the π^* (A_2) resonance, the 90° peak and the d-wave minimum at $\theta = 125^\circ$ are not clear. However, a finer scan of the scattering

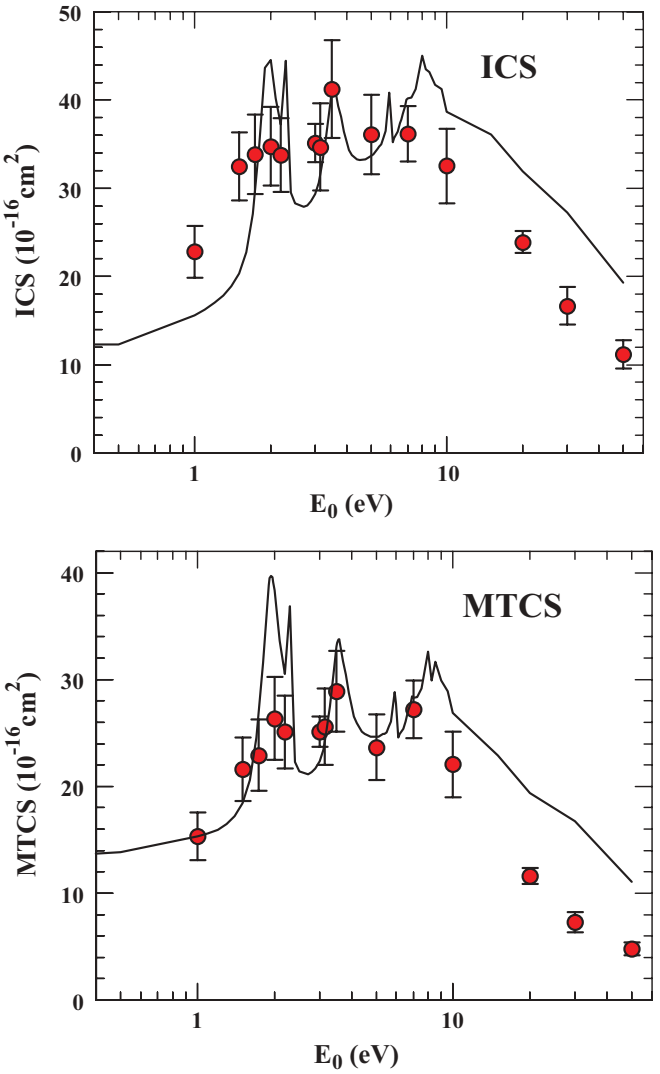

FIG. 3. (Color online) ICS's (top panel) and MTCS's (bottom panel) for furan as a function of E_0. Circles are the present experimental values with 1 standard deviation errors and the solid line is theory, SMCPP with polarization effects.

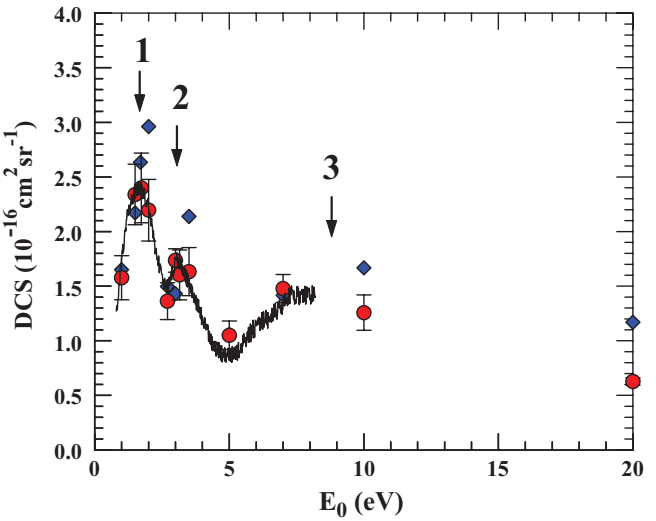

FIG. 4. (Color online) Elastic electron scattering DCS's for furan as a function of E_0 for $\theta = 90^\circ$. Circles are the present experimental DCS's with 1 standard deviation errors. Relative DCS curve at fixed 90° scattering, normalized to 2 eV experimental DCSs; Diamonds are theory, SMCPP with polarization effects. The energy positions of negative ion resonances are labeled with arrows. See text for discussion.

signal versus E_0 for $\theta = 90^\circ$ (solid line in Fig. 4) shows up these resonances in this figure at the E_0 values of (1) 1.7 ± 0.1 eV and (2) 3.1 ± 0.1 eV, with the π^* (A_2) resonance described over a weaker maximum that is almost a shoulder. This weaker characteristic of the π^* (A_2) resonance is also observed in [13]. A broader shape (3) appears to peak at $\approx$8.8 eV, but is not covered in the work of [13].

In Fig. 3, we show ICS's for elastic scattering and MTCS's. The ICS's are experimentally determined by extrapolating our DCS's to small and large scattering angles (θ). At small θ, we used the Born-dipole approximation or theory as a guide, while for large angular extrapolation, we used theory. In this the error induced by extrapolation can be gauged by flat-extrapolating the DCS's to large and small DCS's (see Ref. [26]) and using the deviation as an additional source of error to the average DCS error to make up the total ICS and MTCS uncertainties. A comparison between the theory and experiment shows excellent overall agreement at low E_0 values. As mentioned previously, at E_0 values above 7 eV, theory stays higher because of the fact that excitation and ionization channels become more significant (e.g., at $E_0 =$ 20 eV), the theory is about 30% higher than experiment, providing an estimate of the importance of these channels, which will be a future subject of investigation in this collaboration. The numerical values of the present experimental cross sections are listed in Table II for energies up to 50 eV. Theoretical ICS's obtained in the SEP approximation and shown in Fig. 3 indicate the presence of two prominent resonant peaks located at 1.95 and 3.56 eV which, from the symmetry decomposition of the ICS's, are assigned to the B_1 and A_2 symmetries of the C_{2v} group, respectively. The position of these resonances is consistent with present experimental predictions and also with previous electron transmission measurements performed by Modelli and Burrow [13]. Although not shown here, these structures are strongly sensitive to the inclusion of polarization effects and we observed a shift in their maximum peaks to lower energies, as expected, by an amount of $\sim$2 eV in going from SE to SEP calculations. Sharp-peaked structures appearing in our calculated ICS results around 2.3 and 5.9 eV (the second and fourth structures) were found to be unstable under numerical analysis and were therefore considered as spurious. Above 7 eV our ICS's show another broad structure that is a result of a superposition of pseudoresonances due to closed channels that should be open at those energies. Momentum transfer cross sections obtained in the SMCPP calculations at the SEP level follows basically the same trends of the elastic ICS's.

We also carried out small basis set calculations using GAMESS to look at the lowest unoccupied molecular orbital (LUMO) and LUMO + 1 orbitals. We used the 6–31(d) basis set at the Hartree-Fock level to optimize the molecular ground-state geometry and to diagonalize the Fock operator. We also employed an empirical formula [41], which has been used by experimentalists [13] with success to estimate the

TABLE II. Experimental elastic electron scattering DCS's for furan at various E_0 values and associated errors. Units are 10^{-16} cm^2/sr. Bottom two rows are ICS and MTCS values with associated uncertainties. Values in italics (without errors) are interpolated or extrapolated (using theory) for the purpose of integrating the DCS's to obtain ICS's and MTCS's. The errors are shown in parentheses.

E_0 (eV) → Angle (deg)↓	1 eV	1.5 eV	1.73 eV	2 eV	2.7 eV	3 eV	3.15 eV
0	*58,800*	*88,300*	*10,200*	*4000*	*300*	*300*	*300*
5	*68.5*	*100*	*100*	*40*	*40*	*40*	*40*
10	*14*	*20.0*	*20*	*15*	*15*	*15*	*15*
15	*7.3*	8.87(1.15)	7.78(1.04)	8.86(1.48)	*8.1*	8.59(1.31)	8.89(1.36)
20	4.05(0.55)	5.48(0.67)	4.90(0.73)	6.62(0.88)	5.55(0.82)	6.43(0.10)	6.47(0.97)
25	2.87(0.37)	3.31(0.42)	4.02(0.55)	4.69(0.60)	4.09(0.59)	5.40(0.38)	5.43(0.80)
30	2.28(0.32)	2.36(0.32)	2.99(0.38)	3.92(0.51)	3.94(0.55)	4.78(0.25)	4.58(0.66)
40	1.28(0.17)	1.82(0.24)	2.23(0.32)	3.15(0.43)	3.63(0.53)	3.94(0.35)	3.80(0.54)
50	1.05(0.13)	1.78(0.22)	2.18(0.28)	3.00(0.40)	3.89(0.52)	3.65(0.33)	3.30(0.45)
70	1.41(0.18)	2.46(0.31)	2.42(0.32)	2.83(0.37)	2.70(0.37)	2.83(0.21)	2.73(0.39)
90	1.58(0.20)	2.34(0.28)	2.40(0.32)	2.20(0.28)	1.36(0.17)	1.74(0.11)	1.60(0.23)
110	1.44(0.21)	1.57(0.22)	1.51(0.22)	1.49(0.22)	1.24(0.17)	1.34(0.07)	1.48(0.21)
130	0.946(0.147)	1.30(0.20)	1.27(0.26)	1.51(0.21)	1.71(0.23)	1.65(0.14)	1.77(0.25)
140	*0.90*	*1.2*	*1.3*	*1.75*	*2.2*	*1.9*	*2.0*
150	*0.85*	*1.3*	*1.6*	*2.2*	*2.5*	*2.2*	*2.3*
160	*0.82*	*1.4*	*2.0*	*2.8*	*2.8*	*2.4*	*2.6*
170	*0.80*	*1.5*	*2.5*	*3.8*	*3.2*	*2.6*	*2.8*
180	*0.80*	*1.6*	*2.8*	*5.2*	*3.4*	*2.6*	*3.0*
ICS	22.8(2.9)	32.5(3.8)	33.9(4.5)	34.7(4.5)	33.8(4.2)	35.1(2.2)	34.7(4.9)
MTCS	15.3(2.2)	21.6(3.0)	22.9(3.4)	26.4(3.9)	25.1(3.4)	25.1(1.4)	25.6(3.6)

Energy (eV)→ Angle (deg)↓	3.5 eV	5 eV	7 eV	10 eV	20 eV	30 eV	50 eV
0	*300*	*100*	*80*	*30*	*70*	*60*	*45*
5	*48*	*40*	*36*	*25*	*50*	*40*	*35*
10	*23*	*20*	16.9(2.30)	*20*	32.2(3.57)	*28*	*22*
15	13.7(2.0)	12.3(1.4)	11.6(1.39)	16.0(2.51)	22.3(1.33)	16.9(2.1)	12.3(1.5)
20	10.36(1.46)	9.36(1.26)	9.63(1.00)	12.6(1.79)	13.3(0.77)	9.08(1.15)	4.67(0.56)
25	7.95(1.10)	8.58(1.12)	*8.10*	8.71(1.25)	7.41(0.40)	4.38(0.54)	1.92(0.25)
30	5.85(0.77)	6.71(0.90)	5.88(0.68)	7.10(1.02)	3.89(0.25)	2.34(0.33)	1.01(0.12)
40	4.76(0.58)	4.97(0.63)	4.16(0.39)	3.69(0.50)	1.29(0.08)	0.785(0.099)	0.485(0.064)
50	4.01(0.52)	3.96(0.48)	2.76(0.29)	2.17(0.30)	0.639(0.040)	0.546(0.071)	0.401(0.049)
60						0.458(0.052)	0.302(0.039)
70	2.61(0.34)	1.92(0.25)	1.28(0.14)	1.13(0.16)	0.686(0.060)	0.385(0.050)	0.202(0.025)
90	1.63(0.22)	1.05(0.13)	1.48(0.13)	1.26(0.16)	0.628(0.033)	0.345(0.044)	0.185(0.027)
110	1.70(0.22)	1.28(0.17)	2.02(0.20)	1.66(0.23)	0.682(0.044)	0.397(0.051)	0.204(0.026)
120						0.465(0.059)	0.301(0.026)
130	1.97(0.28)	1.68(0.22)	*0.221*(0.20)	1.72(0.23)	0.951(0.048)	0.567(0.068)	0.389(0.048)
140	*2.3*	*2.0*	*2.2*	*1.85*	*1.1*	*0.69*	*0.5*
150	*2.9*	*2.4*	*2.16*	*2.0*	*1.2*	*0.85*	*0.65*
160	*3.2*	*2.8*	*2.4*	*2.3*	*1.4*	*1.0*	*0.78*
170	*3.5*	*3.3*	*2.9*	*2.8*	*1.6*	*1.2*	*0.93*
180	*3.7*	*3.8*	*3.4*	*3.4*	*1.8*	*1.3*	*1.05*
ICS	41.3(5.5)	36.1(4.5)	36.2(3.2)	32.5(4.2)	23.9(1.3)	16.7(2.1)	11.2(1.6)
MTCS	28.9(3.8)	23.7(3.1)	27.2(2.7)	22.1(3.1)	11.6(0.8)	7.30(0.94)	4.80(0.61)

resonance's positions, to scale our computed LUMO and LUMO + 1 energies. Our computed values for LUMO (B_1) and LUMO + 1 (A_2), that are π^* orbitals and are shown in Fig. 5, were 4.88 and 6.82 eV, respectively. Using the empirical formula, these values scaled to 1.63 and 2.91 eV, which are in close agreement with the experimental values of 1.65 and 3.10 eV, respectively. We show in Fig. 5 the plots of these orbitals. Both orbitals are concentrated on the C = C double bonds, the LUMO being concentrated on the entire ring. According to the characteristics of the LUMO + 1, we suggest that the higher π^* (A_2) resonance would be responsible for the formation of the closed shell furanyl anion through the

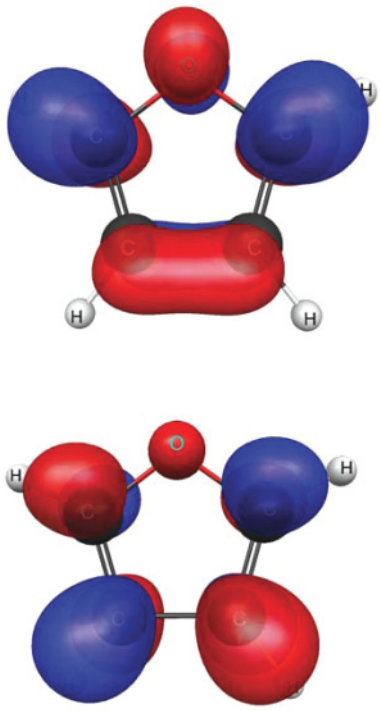

FIG. 5. (Color online): LUMO (top panel) and LUMO+1 (bottom panel) orbitals of furan (generated with MacMolPlot [33]). See text for discussion.

loss of a neutral hydrogen atom. Although based in purely qualitative arguments, such observation presents a straight connection with the experimental findings reported by Sulzer and co-workers. [14] for the dissociative electron attachment (DEA) to furan. Our results for the LUMO, on the other hand, indicate that the lower-lying $\pi^*(B_1)$ resonance can also lead to breakage of the C–C single bond, eventually followed by the decomposition of the furanose ring, though no evidence for the existence of such dissociation pathway was detected in the DEA measurements mentioned previously. In both cases the process would be indirect and should occur through the coupling of π^* and σ^* anions.

V. CONCLUSIONS

We have reported integral, momentum transfer, and differential cross sections for elastic scattering of low-energy electrons by furan, obtained in a joint experimental and theoretical collaboration. Quantitative agreement between theory and experiment is very good, especially for energies below 10 eV. Typical steep raising of the differential cross sections at the forward direction due to the dominant character of the long-range electron-dipole interaction was experimentally observed and theoretically modeled. Differential cross sections were also measured at fixed scattering angles in an attempt to predict the formation of negative-ion resonances. In this respect, our calculated ICS results show two π^* shape resonances located at the energies of 1.95 and 3.56 eV belonging to B_1 and A_2 symmetries, which are in good agreement with the experimental values of 1.65 and 3.10 eV. These findings were further supported by the results obtained by means of a procedure that involves the scaling of the energies associated to the LUMO and LUMO+1 orbitals. The new round of calculations performed in this work provided a better description of polarization effects than our previous study on electron-furan collisions.

ACKNOWLEDGMENTS

This work was sponsored by the US National Science Foundation under Grant Nos. PHY 0653452 (M. A. K., J. M., and K. R.). R. F. da C. and M. A. P. L. would like to acknowledge the financial support from the Brazilian agency Fundação de Amparo à Pesquisa do Estado de São Paulo (FAPESP). R. F. da C., M. H. F. B., and M. A. P. L. would like to acknowledge the financial support from the Brazilian agency Conselho Nacional de Desenvolvimento Científico e Tecnológico (CNPq). M. H. F. B. acknowledges support from the Paraná State agency Fundação Araucária and from Finep (under Project no. CT- Infra). M. H. F. B. also acknowledges computational support from Professor Carlos de Carvalho at DFis-UFPR. The authors acknowledge computational support from CENAPAD-SP and from CCJDR-IFGW-UNICAMP. This work is part of a cooperative project between NSF and CNPq (CNPq under Project No. 490415/2007–5).

[1] B. Boudaïffa, P. Cloutier, D. Hunting, M. A. Huels, and L. Sanche, Science **287**, 1658 (2000); L. Sanche, Eur. Phys. J. D **35**, 367 (2005); F. Martin, P. D. Burrow, Z. Cai, P. Cloutier, D. Hunting, and L. Sanche, Phys. Rev. Lett. **93**, 068101 (2004).
[2] A. Zecca, C. Perazzolli, and M. J. Brunger, J. Phys. B **38**, 2079 (2005).
[3] P. Mozejko and L. Sanche, Radiat. Phys. Chem. **73**, 77 (2005).
[4] C. König, J. Kopyra, I. Bald, and E. Illenberger, Phys. Rev. Lett. **97**, 018105 (2006).
[5] C. Winstead and V. McKoy, J. Chem. Phys. **125**, 244302 (2006).
[6] C. Winstead and V. McKoy, J. Chem. Phys. **125**, 074302 (2006).
[7] D. Bouchiha, J. D. Gorfinkiel, L. G. Caron, and L. Sanche, J. Phys. B **39**, 975 (2006).
[8] C. S. Trevisan, A. E. Orel, and T. N. Rescigno, J. Phys. B **39**, L255 (2006).
[9] C. J. Colyer, V. Vizcaino, J. P. Sullivan, M. J. Brunger, and S. J. Buckman, New J. Phys. **9**, 41 (2007).
[10] M. H. F. Bettega and M. A. P. Lima, J. Chem. Phys. **126**, 194317 (2007).
[11] T. C. Freitas, M. A. P. Lima, S. Canuto, and M. H. F. Bettega, Phys. Rev. A **80**, 062710 (2009).
[12] T. Fleig, S. Knecht, and C. Hättig, J. Phys. Chem. A **111**, 5482 (2007).
[13] A. Modelli and P. W. Burrow, J. Phys. Chem. A **108**, 5721 (2004).
[14] P. Sulzer *et al.*, J. Chem. Phys. **125**, 044304 (2006).

[15] M. H. Palmer, I. C. Walker, C. C. Ballard, and M. F. Guest, Chem. Phys. **192**, 111 (1995).
[16] R. F. da Costa, M. H. F. Bettega, and M. A. P. Lima, Phys. Rev. A **77**, 012717 (2008).
[17] B. C. Ibanescu, O. May, and M. Allan, Phys. Chem. Chem. Phys. **10**, 1507 (2008).
[18] K. Aflatooni, A. M. Scheer, and P. D. Burrow, J. Chem. Phys. **125**, 054301 (2006).
[19] M. Allan, J. Phys. B **40**, 3531 (2007).
[20] S. Tonzani and C. H. Greene, J. Chem. Phys. **125**, 094504 (2006).
[21] F. Blanco and G. Garcia, Phys. Lett. A **360**, 707 (2007).
[22] A. L. McClellan, *Tables of Experimental Dipole Moments* (W. H. Freeman and Co., San Francisco, 1963).
[23] J. J. Oh, K. W. Hillig II, and R. L. Kuczkowski, J. Phys. Chem. **94**, 4453 (1990).
[24] M. A. Khakoo, C. E. Beckmann, S. Trajmar, and G. Csanak, J. Phys. B **27**, 3159 (1994).
[25] J. H. Brunt, G. C. King, and F. H. Read, J. Phys. B **10**, 1289 (1977).
[26] M. A. Khakoo, H. Silva, J. Muse, M. C. A. Lopes, C. Winstead, and V. McKoy, Phys. Rev. A **78**, 052710 (2008).
[27] M. Hughes, K. E. James Jr., J. G. Childers, and M. A. Khakoo, Meas. Sci. Technol. **14**, 841 (1994).
[28] M. Dampc, A. R. Milosavljevi'c, I. Linert, B. P. Marinković, and M. Zubek, Phys. Rev. A **75**, 042710 (2007).
[29] K. Takatsuka and V. McKoy, Phys. Rev. A **24**, 2473 (1981); **30**, 1734 (1984).
[30] M. H. F. Bettega, L. G. Ferreira, and M. A. P. Lima, Phys. Rev. A **47**, 1111 (1993).
[31] G. B. Bachelet, D. R. Hamann, and M. Schlüter, Phys. Rev. B **26**, 4199 (1982).
[32] M. H. F. Bettega, A. P. P. Natalense, M. A. P. Lima, and L. G. Ferreira, Int. J. Quantum Chem. **60**, 821 (1996).
[33] B. M. Bode and M. S. Gordon, J. Mol. Graphics Modell. **16**, 133 (1998).
[34] M. W. Schmidt *et al.*, J. Comput. Chem. **14**, 1347 (1993).
[35] R. F. da Costa, F. J. da Paixão, and M. A. P. Lima, J. Phys. B **37**, L129 (2004); **38**, 4363 (2005).
[36] C. W. Bauschlicher Jr., J. Chem. Phys. **72**, 880 (1980).
[37] Y. Okamoto, K. Onda, and Y. Itikawa, J. Phys. B **26**, 745 (1993).
[38] H. Cho, Y. S. Park, E. A. y Castro, G. L. C. de Souza, I. Iga, L. E. Machado, L. M. Brescansin, and M.-T. Lee, J. Phys. B **41**, 045203 (2008).
[39] L. M. Brescansin, L. E. Machado, M.-T. Lee, H. Cho, and Y. S. Park, J. Phys. B **41**, 185201 (2008).
[40] R. H. Read, J. Phys. B **1**, 893 (1968).
[41] S. W. Staley and J. T. Strnad, J. Phys. Chem. **98**, 116 (1994).